Journal of the Optical Society of America A
OPTICS, IMAGE SCIENCE, AND VISION

Wide-range adaptive optics visual simulator with a tunable lens

Nikolai Suchkov,[1,2] Enrique J. Fernández,[1,*] and Pablo Artal[1]

[1]Laboratorio de Óptica, Centro de Investigación en Óptica y Nanofísica (CiOyN), Universidad de Murcia, Campus de Espinardo, 30010 Murcia, Spain
[2]Voptica S.L., Parque Científico de Murcia, Ctra. de Madrid 388, Complejo de Espinardo-Edificio S, 30100 Murcia, Spain
*Corresponding author: enriquej@um.es

Received 15 November 2018; revised 12 March 2019; accepted 19 March 2019; posted 20 March 2019 (Doc. ID 352061); published 4 April 2019

An adaptive optics visual simulator (AOVS) with an extended dioptric range was developed, allowing measuring and correcting aberrations in a majority of highly ametropic eyes. In the instrument, a tunable lens is used for defocus correction, while a liquid-crystal-on-silicon spatial light modulator is used for compensating or inducing any other aberration. The instrument incorporates a digital projector, which uses a micromirror array to display the stimuli. A motorized diaphragm enables operation for any physiological pupil size. A full description of the instrument and its calibration are provided, together with the results obtained in seven highly myopic subjects with refraction of −7.2 ± 1.8 D (mean ± SD). Refraction obtained with the instrument was compared to the standard refraction prescribed by trial lenses. When using the refraction obtained by the AOVS, the visual acuity (VA) exhibited an average increase of 0.21 (decimal scale). The visual impact of correcting high-order aberrations is presented in three subjects, whose VAs slightly improved with the correction. High myopes are able to benefit from the improved refraction assessment. The new instrument creates a possibility for a wide number of new experiments, especially for eyes exhibiting large refractive errors, where previous AO instruments failed to operate.

https://doi.org/10.1364/JOSAA.36.000722

1. INTRODUCTION

Human vision is a complex system, involving both optics of the eye and the neural system. The brain interprets the information about the received image for the final perception of the scene. Each step of the process is equally important, deserving a thorough characterization. However, the first limitation of human vision arises from optical aberrations of the eye, which manifest in a degradation of the retinal image as compared to the perfect diffraction-limited image. The most significant aberration in the human eye (in terms of amplitude) is defocus, resulting in myopia or hyperopia, depending on its sign. In particular, myopia has become a rising concern in the last years, with the so-called "epidemic" of myopia. A higher prevalence of myopia is seen in some Asian countries [1–3]. Due to this, precise refraction assessment and characterization of the optics of such eyes is a topic of highest interest.

Nowadays, the most widely used method to characterize the optics of the eye is a Hartmann–Shack wavefront sensor (HS) [4–6]. Since its first applications at the end of the last century, the method has been successfully employed in a large number of studies [7–12]. However, knowing the optical quality of the eye is not enough to fully characterize vision. Visual testing must be performed in order to get a complete picture, including the neural and perceptual stages of the process.

As the development of the HS in vision was going on, adaptive optics (AO) techniques were applied for the study of the eye. This modality allows to measure and manipulate aberrations. Although initially developed for astronomical applications, AO techniques have been successfully applied to better understand retinal morphology and the function of the eye [13–20]. One of the applications of AO is visual simulation. AO visual simulators (AOVS) enable better understanding of the aberrations' impact on vision [21–24]. These systems combine both objective retrieval of the ocular aberrations and visual testing to understand the correlation between optical and visual quality. The wavefront formed by the stimulus is modulated by inducing or compensating aberrations to evaluate their effect on vision [25–33].

Some of the current AOVS exhibit one major drawback: the limited refraction range that can be measured and corrected. Due to this, for patients exhibiting high myopia, for instance, trial lenses must be placed at the entrance of the AO system. It becomes paradoxical that such a sophisticated instrument still requires trial lenses for pre-compensating a large defocus. This happens mainly because of the limited amplitude in phase

modulation that can be achieved by deformable mirrors [15–19], or liquid-crystal-based spatial light modulators (SLMs) [23,24,34–36]. The latter typically operate with phase wrapping, with the range of operations being limited by the pixel size. However in practice, their amplitude is limited due to diffraction effects associated with a large amount of phase wrapping [21]. This drawback affects the performance of AO instruments, particularly when they are intended for patients with high myopia.

In this work, we present a novel instrument that is able to solve the problem of limited range by dividing the task of aberration modulation between a liquid-crystal-on-silicon SLM (LCoS-SLM) and a tunable lens (TL), allowing to extend AOVS technology to highly aberrated eyes.

2. METHODS

A. Overview

The instrument is depicted in Fig. 1. Wavefront manipulation was accomplished by using two different devices: a LCoS-SLM, (PLUTO-VIS-014, Holoeye Photonics AG, Berlin, Germany) and an electrically TL (Optotune EL-16-40-TC-VIS-20D, Optotune Switzerland AG, Dietikon, Switzerland). The instrument was compounded by two optical relays. The measurement

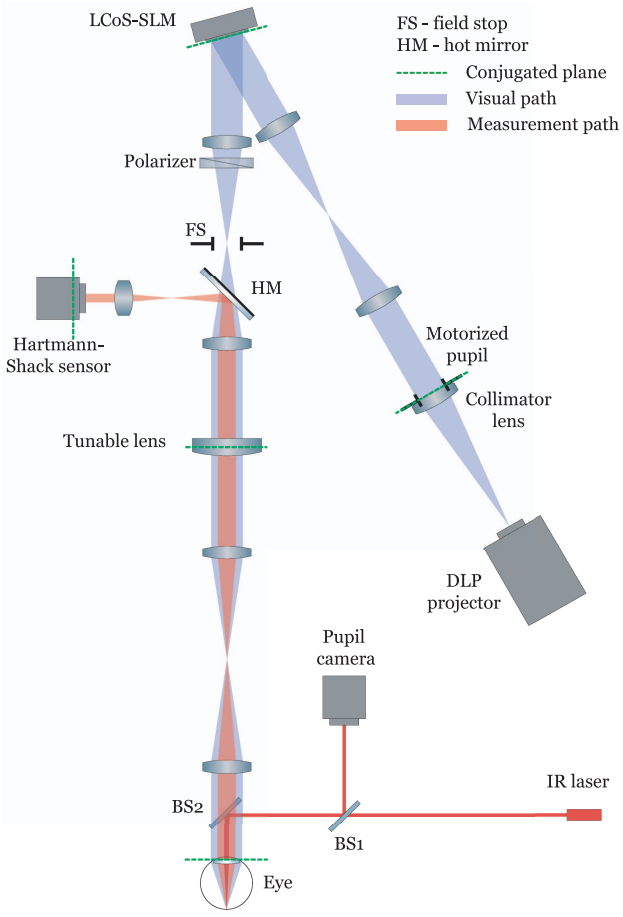

Fig. 1. Schematic of the new adaptive optics visual simulator with an extended dioptric range. BS1, BS2, beam splitters; FS, field stop; HM, hot mirror; L1 to L7, achromatic doublets. Figure not to scale. Further description of the elements is provided in the main text.

relay (red color in Fig. 1) allowed the HS sensor to evaluate the wavefront. The visual relay (blue color in Fig. 1) displayed the stimuli through the manipulated or corrected optical conditions. The LCoS-SLM was used only in the visual relay, while the TL operation affected both relays.

The measurement relay was equipped with a laser diode (IR laser in Fig. 1) emitting at 780 nm producing a point-like aerial image on the retina, which acted as a reference beacon for the HS wavefront sensor. The axial position of the subject was adjusted with the help of a linear translation stage and a camera (pupil camera in Fig. 1) focused at the exit pupil of the system. Once aligned, the pupil of the eye was conjugated optically to the plane of the TL, and then onto the HS by using telescopes. A hot mirror (HM in Fig. 1) guaranteed that only IR light was sent to the wavefront sensor, while visible light from the visual relay passed through, in the direction of the eye. The TL enabled pre-compensation of the defocus of the wavefront coming from the eye of the subject. One of the TL's surfaces is a thin elastic polymer membrane. A liquid material is contained inside. A circular electrode ring is located on top of the elastic membrane, which is either pushed or pulled depending on the applied voltage. The net effect is the change in the membrane's curvature, making it either convex or concave. The TL has a nominal defocus range of ± 10 D, and a usable aperture of 16 mm. The lens has a temperature sensor, allowing precise defocus generation under changing thermal conditions. Using the TL significantly flattened the wavefront, as defocus is typically the dominant aberration of the eye. This is particularly important for ametropic eyes showing high refraction values. Correction of defocus enhances precision of the HS, as it allows to limit the displacement of the spots on the sensor, well within the linear range of the HS. The dynamic range of the HS is imposed by both the dimensions of a cell and the focal length of the microlens array [37]. A custom HS sensor was built using an off-the-shelf microlens array with a focal length of 3.17 mm (APO-Q-P192-F3.17, Flexible Optical B.V., Rijswijk, Netherlands), with control software developed in C. The program estimated Zernike polynomials in order to describe the wavefront for different pupil sizes. Although HS measurements were done using IR light, visual simulation was done in visible light. To account for this, a defocus shift was introduced. The longitudinal chromatic aberration of the human eye between IR and visible range was considered [26,38].

The visual relay included a high-definition digital-light-processing projector (DLP projector in Fig. 1) (DLPDLCR4710EVM-G2, Texas Instruments, Texas, USA). The projector uses a digital micromirror device (DMD), which is an array of highly reflective aluminum micromirrors that have "on" and "off" states, depending on the angle to the illuminating beam. In the on state, a single micromirror reflects the light into the optical path, while in an off state it reflects it away from the optical axis. Any intermediate gray level is attained by combining on and off states at corresponding frequencies. The projector was disassembled to expose the internal micromirrors, avoiding the projecting optics. The micromirrors operated as the object of the visual simulation system. The micromirror array had a 1920×1080 resolution, with the diagonal of 0.47″ (11.9 mm) and a pixel size of

5.4 μm. The illumination of the micromirrors was done internally by three different LEDs corresponding to R, G, and B channels, providing a total luminous flux of up to 600 lm. The projector provided a possibility for fully photopic vision testing at 30 Hz.

The micromirrors inside the DLP projector were then collimated by an achromatic doublet lens with a focal length of 200 mm. This configuration resulted in an angular pixel size of 6 arc s, allowing psychophysical measurements of visual acuity (VA) with high sampling. The entrance pupil of the system, a motorized diaphragm (8MID8.2-0.8-N, Standa Ltd, Vilnius, Lithuania), was located as close as possible to the collimator lens. The diaphragm could be remotely controlled from a PC, with a diameter range of from 0.8 mm to 8.2 mm, covering the physiological diameters of the human eye. For the purposes of the presented experiment, the pupil diameter was fixed at 4.5 mm.

The entrance pupil was then relayed by a telescope to the LCoS-SLM. The LCoS-SLM had a full HD resolution (1920 × 1080 independent squared pixels of 8 μm side), assembled on a diagonal of 0.7″ (17.8 mm), with a fill factor of 93%. The LCoS-SLM consisted of a parallel-aligned nematic liquid crystal layer sandwiched between a transparent electrode and a silicon wafer with an etched array of pixels. The phase modulator was controlled by sending images from the computer. The gray-level images shown on the LCoS-SLM induced a phase retardation on the incoming wavefront. A field stop (FS in Fig. 1) limited the size of the object, while also filtering the diffraction effects associated with the pixilation of the LCoS-SLM. The wavefront was then relayed to the TL, where defocus was added independently from the LCoS-SLM. Defocus was controlled from the readouts of the HS or directly from subjective adjustments driven by the patient. All the telescopes in the system were made of achromatic doublet lenses, keeping a magnification of 1 between the eye and the plane of the collimating lens. The field displayed to the subject subtended an angular size of 3.1 by 1.7 deg.

B. Calibration

The system required precise alignment and calibration to assure optical conjugation across different pupil planes, as shown in Fig. 1 with green dashed lines. For calibration of the measurement relay, an auxiliary collimated beam from a He–Ne laser emitting at 542.8 nm was introduced in the optical system following the IR laser diode path. The parameters of the HS sensor were also obtained experimentally. The effective focal length of the lenslet array was 2.75 mm.

The TL had to be calibrated in order to attain an accurate control of the defocus, as the relationship between input current, and generated optical power was not linear in the device. The variable lens was calibrated once mounted in the AO system. A set of current signals was sent to the TL, with the associated defocus values measured by the HS. The TL exhibited a significant hysteresis. Consequently, the achieved defocus depended on the previous defocus, in addition to the applied signal. Figure 2 shows the response of the TL to different sequences of input signals, illustrating the effect of hysteresis. Four sequences are shown: for sequences A and B, the input current was changed from −180 mA to 180 mA and in opposite directions, in steps of 20 mA; for sequences C and D, current was reset to the values 220 mA and −220 mA, respectively. Hysteresis exhibited a maximum value of 1.3 D, which is relevant for ophthalmic applications [39].

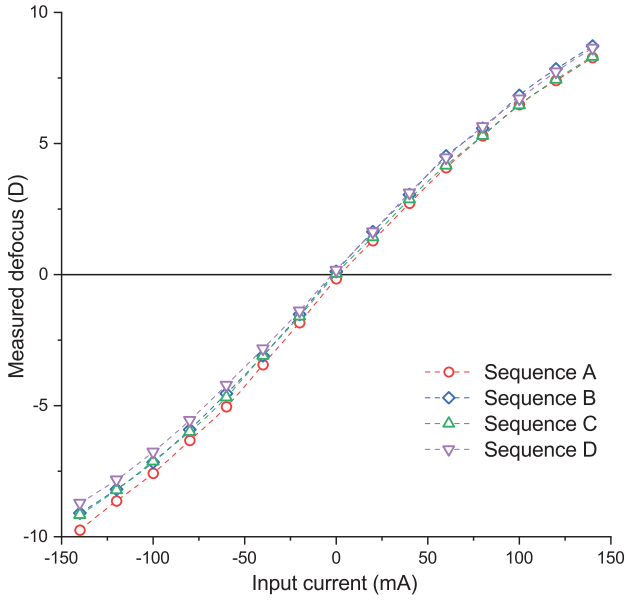

Fig. 2. Hysteresis exhibited by the TL. Maximum difference between different operation sequences reached 1.3 D at −140 mA. Sequence descriptions can be found in the text.

For precise control of the TL, an alternative protocol for calibration was devised. A set of 1000 random input signals was applied to the lens, retrieving the corresponding values of defocus with the HS. Those were employed to fit a polynomial function by applying a least squares curve-fitting algorithm. The obtained polynomial function was then taken as the control function to drive the TL. The procedure is robust and collaterally provides the standard deviation, which in our case was 0.11 D, as an estimator of the uncertainty existing between the programmed and experimental values of defocus. The error of 0.11 D is negligible for visual applications, since its effect on the perceived image would be unnoticeable [39]. The range of use for the TL after calibration spanned from −12 D to 10 D.

The left panel in Fig. 3 shows the actual control function used in the instrument after calibration. Another source of

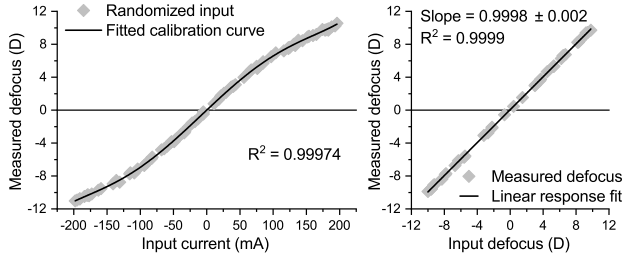

Fig. 3. TL calibration. Left panel: defocus modulation curve for random pattern. Right panel: response of the TL after calibration. See text for more information.

uncertainty in the TL arises from its internal temperature. Multiple calibration curves were obtained, with each one having a different temperature. The measurements showed that the effect of the temperature was linear, with a deviation in optical power of 0.033 D over 1 deg. Celsius variation. The right panel in Fig. 3 shows the response function of the TL after calibration.

It should be noted that due to the non-neglectable thickness of the TL, and the change in its shape produced by the magnitude and sign of the programmed defocus, the position of the principal planes also varies accordingly. The largest change occurs when the lens changes from a plano-concave to a plano-convex profile. Simulations of the displacement of the principal planes as a function of defocus were done using ray-tracing software (Zemax, LLC, Washington, USA). A maximum shift of 4 mm between limit positions of the TL was found. Those were naturally included in the calibration curve, as they were obtained by the HS sensor, whose plane remained fixed. Figure 4 shows the TL in three different states, producing negative power, no power, and positive power.

Regarding the chromatic dispersion of the TL, the supplier specifies a value of Abbe number of 108.49 for the contained fluid. Therefore, especially for visual applications, the lens can be considered achromatic. As an example, when modulating defocus of 5 D, the TL produces a total chromatic shift of 0.052 D for the considered visible spectrum (450 nm to 630 nm). When experimentally measured, no difference in defocus was found for extreme wavelengths for defocus values of up to 7 D, as the smallest step of the TL was 0.1 D. The optical quality of the lens was also measured with the help of the HS wavefront sensor. A vertical coma aberration was found to be the most substantial, as shown by the Zernike polynomials expansion in Fig. 5, for a pupil diameter of 4.5 mm. Vertical coma arises because of the gravitational attraction affecting the fluid and the flexible membrane. Value of the vertical coma aberration reached 0.053 μm, which is less than the average coma aberration amplitude found in the normal human eye (-0.082 ± 0.069 μm for a 5 mm pupil [40]). This value of coma aberration produced no effect on the VA for the pupil size used in the experiment, as was tested by VA measurements with and without the tunable lens. The aberrations were

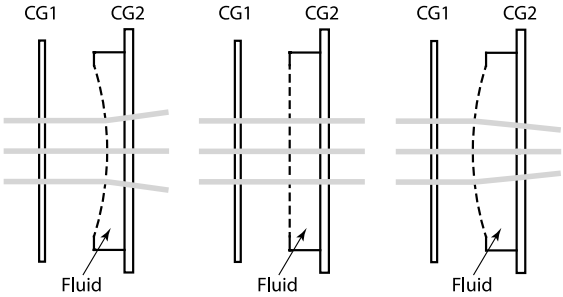

Fig. 4. Three states of the TL. Left panel shows lens producing negative power, middle panel zero power, and right panel positive power. The membrane surface of the lens is shown as a dashed line. CG1 and CG2: cover glasses 1 and 2 enclosing the lens. Gray lines: rays propagating through the lens. The angle of refraction is exaggerated for visual clarity.

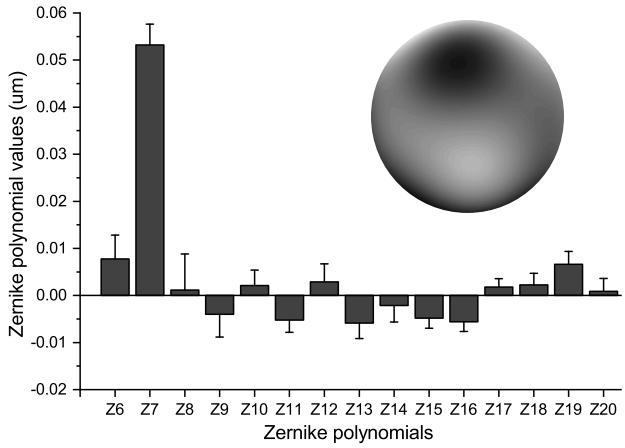

Fig. 5. Zernike polynomials in μm for high-order aberrations (HOA) produced by the TL in OSA ordering for 4.5 mm pupil. Data were averaged from 1000 random defocus values. In the top right corner, the wavefront calculated from the average Zernike polynomial values is shown, scaling from 0 to 2π. Z7 coefficient corresponds to vertical coma aberration.

retrieved in the full range of operation of the TL. The error bars in Fig. 5 show the standard deviation.

The LCoS-SLM was calibrated to assure a linear phase response. The linearization process consisted of determining the relationship between the input signal encoded as a gray level and the generated phase shift. The device was operated as a regular display from the computer. Due to that, the gamma curve could be modified so that the phase modulation response was linear and attained at least 2π. The experimental procedure to linearize the modulator has been described in detail elsewhere [41]. Briefly, this method uses the LCoS-SLM to simultaneously create a plane wavefront whose phase can be varied, and a tilted version of the wavefront with a constant phase value. Both wavefronts interfere in the open space, where a camera records the interference fringes. The phase response is characterized as a function of gray levels from the shift of the interference fringes. A least squares linear fit of phase retardation as a function of gray level produced a correlation coefficient above 0.99, with the total phase modulation equal to 2.0056π.

The alignment of the pupil modulated on the LCoS-SLM and the entrance pupil of the optical system had to be set digitally in order to attain the best possible performance. Any mismatch between the pupils would cause some amount of light with uncontrolled phase to pass through the system. To assure good centering, a procedure was devised. Some amount of defocus aberration was first set to the modulator. An auxiliary camera obtained the images displayed in the projector after phase modulation of the wavefront. The degradation of the defocused image was then characterized by a single parameter, which was the peak value of the energy received on the camera. This peak value was recorded as a function of the position of the phase mask generated at the modulator. The maximum spread of energy, corresponding to minimum peak energy, corresponds to the situation where the pupils are perfectly aligned, as any other configuration would allow a portion of the incoming light

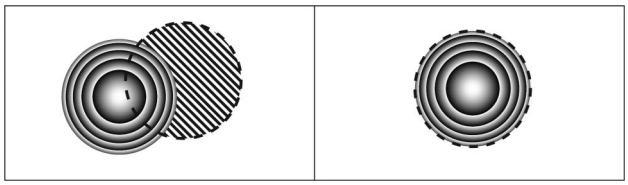

Fig. 6. LCoS-SLM centering. Left frame: LCoS-SLM is not aligned with the physical pupil (shown as oblique fringes); non-modulated light forms focused image on the detector. Right frame: LCoS pupil (shown as a diffractive lens) perfectly coincides with the physical pupil (shown as dashed circle); 100% of the light is modulated.

to be focused on the detector. The procedure is graphically shown in Fig. 6. A similar method was applied to set the polarization of the incoming light. A linear polarizer was rotated until the effect of the programmed defocus by the modulator over the image recorded on the camera was at its maximum level.

The software to perform the required calibrations was written in MATLAB (Mathworks, Natick, MA, USA). To control the experimental setup, software was developed using C++. The program enabled the control of every function of the system from a single computer through a graphical user interface (GUI) adapted for clinical use.

C. Subjects and Visual Acuity Estimation

Seven young adults with mean age of 23.5 (SD = 2, range = 21–27) participated in the measurements. No selection of candidates was done, but a general request of healthy subjects with moderate and high myopia was done among students having some connection to the laboratory. The left eye was measured and used for visual testing for all subjects, except subject S3, in whose case the experiment was done using the right eye (due to the unusually low VA value of 0.5 decimal in the left eye). They exhibited mean spherical refractive error of -7.2 ± 1.8 D, and astigmatism of -1.0 ± 1 D. Natural vision was tested with no cycloplegics instilled at any time. The subjects were informed about the purpose of the experiment, and they signed written consents to participate in the measurements.

The VA was measured in the system using a Freiburg test [42,43] with three repetitions of 90 trials under different visual conditions. Each trial showed a tumbling E letter with one out of four different orientations. Measurements were taken in 100% contrast, with black letters on a white background, using the DLP projector as a stimuli generator. Luminance at the pupil plane was 60 cd/m^2. Entrance pupil of the system was set to 4.5 mm. Subjects' pupils were monitored with a pupil camera during the measurements to ensure the correct alignment. Pupil size was monitored in real time as well. It was above 4.5 mm diameter in all cases. Participants indicated the orientation of the letter by using a keyboard while looking through the system. The raw data from their responses (letter size in arc min and the recoded answer, whether correct or not) as provided by the Freiburg test program were then analyzed using custom software written in MATLAB (Mathworks, Natick, MA, USA). A Boltzmann sigmoid function was fitted for VA determination. The bottom asymptote of the sigmoid was set at 0.25, which is a statistical possibility of guessing the correct orientation when having four choices. The threshold for VA was set at 75% of the correct answers, while the slope in the sigmoid fitting was set as a variable.

3. RESULTS

A. AO-Guided Refraction

Subjects were aligned in the system, ensuring correct lateral and axial position and then stabilized by using a chin rest. The correct positioning of the eye's pupil was monitored in real-time during the runs. A pupil camera operating at video rate (30 Hz) continuously recorded the pupil, illuminated by an IR array of LEDs emitting at 780 nm. The pupil of the eye was optically conjugated to the HS and the TL planes.

Initially, the instrument was used to obtain the refraction of the subjects. The subjects also reported their current refraction [prescribed R_x], as obtained by using trial lenses by a professional optometrist (different for each subject, obtained within the past two years). Given that the reported refraction was intended for ophthalmic lenses, a calculation was carried out to use those values at the eye's exit pupil plane to account for the distance from the eye to an ophthalmic lens, using Eq. (1):

$$D_p = \frac{D_l}{(1 + d \cdot D_l)}, \tag{1}$$

where D_p is the defocus in the pupil plane, D_l is the defocus in the plane of the ophthalmic lens, and d is the distance between those planes.

Defocus and astigmatism from the wavefront measured by the HS sensor were used to calculate the equivalent sphere [measured R_x]. The latter from the first measurement was compensated by the TL. The correction of the equivalent sphere is particularly important for eyes showing high refraction, as it allowed the HS sensor to operate in a linear regime [37]. A second measurement was taken with the HS through the correction of the equivalent sphere. Remaining astigmatism was then compensated by the LCoS-SLM.

Subjects were allowed for further visual refinement of the defocus and astigmatism with the help of a Maltese cross subtending 1 arc minute displayed on the projector. In all cases, the final value after subjective refinement did not deviate more than 0.2 D from the objective estimation retrieved by the HS. Measured values of defocus and astigmatism are shown in Table 1.

Once the low-order aberrations were estimated with the instrument, the impact of correcting the new values over VA was investigated. The results are shown in Fig. 7. Prescribed refraction accounts for recalculation of the values as described previously in Eq. (1).

As seen in Fig. 7, in all cases, an increase in VA was found. Average VA values were 1.00 ± 0.23 for prescribed refraction, and 1.21 ± 0.14 for refraction measured with AOVS. For subjects S2 and S4, the average difference between the VA obtained from the two methods surpassed a paired t-test with P-value lower than 0.05.

Table 1. Comparison between Prescribed Refraction Achieved with Trial Lenses and Measured Refraction Using AOVS[a]

	Trial Lenses		AOVS	
Subject	Sphere	Cylinder	Sphere	Cylinder
S1	−10	–	−10.6	–
S2	−4.2	−4.65 × 175°	−5.2	−4 × 175°
S3	−9	–	−8.8	−1.5 × 170°
S4	−7.5	–	−7.1	−2.2 × 175°
S5	−7	−0.5 × 30°	−7.6	−0.6 × 0°
S6	−7	–	−7	−0.5 × 30°
S7	−5.5	–	−5.5	−0.6 × 45°

[a]Sphere and cylinder values are given in diopters.

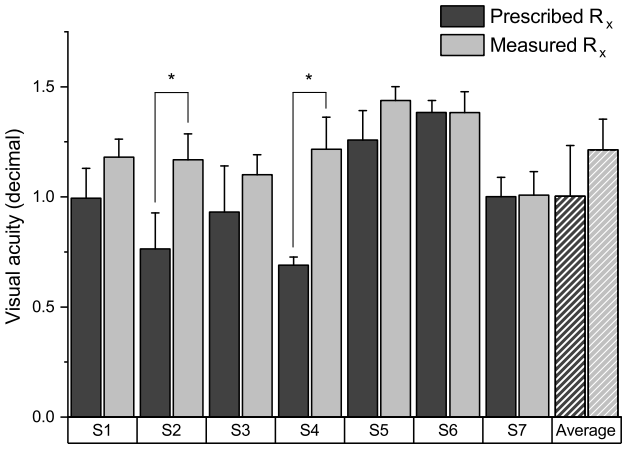

Fig. 7. Comparison of VA achieved by subjects. Prescribed R_x shows VA when correcting prescribed refraction found with trial lenses. Measured R_x shows VA when correcting refraction found using the wavefront measurements by AOVS. Error bars show standard deviation. Asterisks mark statistically significant difference ($P < 0.05$).

B. Compensation of High-Order Aberrations

The system was also tested for compensation of HOA. In this case, stabilizing the subject during the measurements became critical, as even small misalignments can significantly vary the HOA. The subjects were fixed to the system by using their previously taken dental impression. The procedure was carried out on three subjects (S5, S6, and S7) from the set of volunteers, those willing to participate in this additional experiment. The procedure to measure and correct low-order aberrations was repeated as described in the previous section. This time, full aberration correction up to the sixth order was also included after defocus and astigmatism compensation (refraction + HOA). HOA were corrected by the LCoS-SLM. Figure 8 provides some information about the HOA from the three subjects, once defocus and astigmatism were corrected. The top row shows the wavefront 2π wrapped at 550 nm. At the bottom, corresponding point-spread functions (PSFs) and associated Strehl ratios are presented.

The level of HOA in the three subjects is within the normal range for emmetropes and low myopes [40], although the individual variability is quite high, as shown by the Strehl

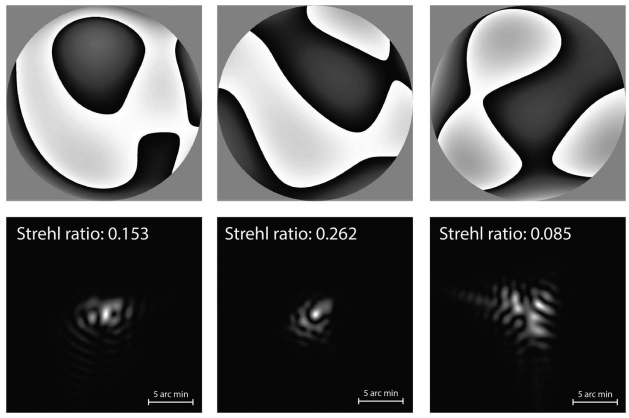

Fig. 8. Optical quality measurements, with only high-order aberrations included. From left to right: subjects S1, S2, S3. Top row: wavefronts, 2π wrapped. Bottom row: Point-spread functions (PSFs). Corresponding Strehl ratios are shown in the top left corner of PSF images.

ratios. VA values were obtained for this group to compare correction of low-order aberrations with correction of all aberrations up to sixth order. The results are shown in Fig. 9. In all cases, correction of HOA results in a superior VA in comparison to low-order aberration correction. Even in subjects with higher VA, S5 and S6, the correction of HOA shows a benefit in the VA. Subject S7, whose refraction was lower, 5.5 D versus 7 D for the other two subjects, and whose Strehl ratio showed a higher amount of HOA, attained the lowest VA after correction.

For all seven subjects, full information about their optical aberrations was retrieved. Defocus and astigmatism were fully corrected, according to the average of three HS measurements. The residual error for a pupil of 4.5 mm is shown in Fig. 10, superimposed on the data for normal population for comparison purposes. The data for normal population are adapted from

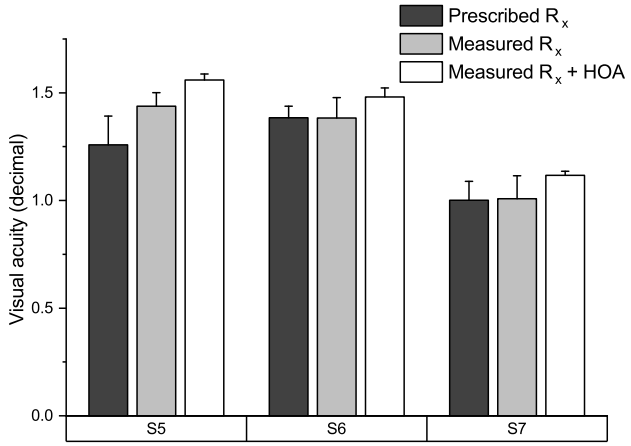

Fig. 9. Comparison of achieved VA when correcting only low-order aberrations (trial lenses refraction and AO-guided refraction) and when correcting all Zernike polynomials up to sixth order (AO-guided refraction + HOA). Error bars show standard deviation.

Fig. 5 from a different study [40]. The measured RMS wavefront error is within the range expected for normal population.

4. DISCUSSION AND CONCLUSION

The instrument described in this work extends the application of AO for visual simulation to patients with large amounts of defocus without compromising the retrieval and correction of HOA. The estimation of the refraction from wavefront measurements was very accurate in all cases. Subjective refinements barely changed the final values of equivalent sphere, as the difference was below 0.2 D, which is within the depth of field for the considered pupil size. Relative compactness of the instrument combined with easy-to-use software permits the usage of the system in a clinical environment, reducing the workload for optometrists.

A more precise estimation of HOA is possible due to the defocus being compensated before the HS, leading to a better characterization of the optics of a highly myopic eye. To showcase this, the average RMS of the HOA from the seven subjects was compared with the existing data obtained in larger populations. Figure 10 shows the average RMS error for measured high myopes (hollow circle) and for normal population, as was reported by Salmon *et al.* [40].

Some measurements of optical aberrations in high myopes have shown that their HOA RMS is similar to that found in near-emmetropic population [40,44,45]. However, some other studies have found that HOA RMS increases as a function of the myopic refractive error [46,47]. The question seems to be open for further studies. In the present work, only seven subjects were measured, all of them young adults. The limited number of subjects prevents making a definitive conclusion, though the results are more in the direction of showing a similar level of HOA for the 4.5 mm pupil. Previous works [46] found that the RMS increase in high myopes is more substantial for larger pupils. In spite of the reduced number of subjects, the HS measurements were done after a pre-compensation of equivalent sphere, which ensures a higher accuracy [37] in the estimation of HOA as compared to previous studies [46–49].

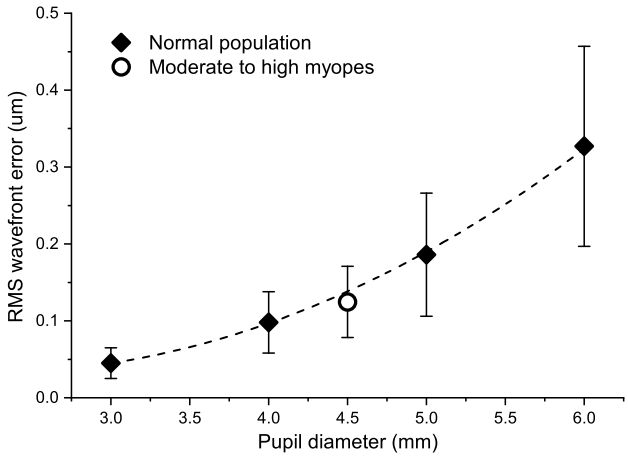

Fig. 10. Average RMS wavefront error for seven measured subjects (hollow circle). Error bars indicate standard deviation. Data for normal population (filled rhombus) are taken from a different study [40].

The AOVS presented in this work offers additional advantages, since the LCoS-SLM provides the possibility of inducing virtually any phase. It can be employed to evaluate the performance of any optical correction, in addition to regular ophthalmic lenses, including multifocal, and diffractive profiles. The instrument allows the evaluation of any optical solution under any physiological pupil size and luminance condition.

The implementation of the TL with a large defocus range helps to reduce phase-wrapping effects [21], since the LCoS-SLM does not have to correct defocus, which typically is the most prominent aberration. Severe phase wrapping typically reduces contrast because of the energy spread produced by diffraction. TLs have been used in visual optics [50], as well as for eye imaging [51,52]. However, to the best of our knowledge, they have not been yet combined with the LCoS-SLM for separating defocus modulation from HOA modulation.

Driving defocus with the lens also enables for much faster control of this aberration, which can be corrected in real time, while SLM can do a static or slower compensation for the rest of the wavefront. Additionally, the TL allows a true closed-loop operation, as the effect of defocus manipulation can be retrieved by the sensor. This is typically not possible with the LCoS-SLM, as it is designed for a limited wavelength range. Consequently, performing visual testing in visible light prevents the simultaneous use of the LCoS-SLM in the IR, where aberrations are typically obtained.

The working range of the TL can be shifted by acting in the optics of the system, or even simpler, by changing the position of the object with regard to the collimating lens. The ± 10 D range can be, for instance, shifted to $[-15, 5]$ D, since hyperopic eyes above this value are seldom found. However, high myopia, defined for refraction of < -5 D [53], does have a much higher prevalence, around 3% of the global population.

The motorized iris at the entrance pupil further extends the flexibility of the instrument, as it makes it possible to enforce any pupil size for simulating different optical conditions, e.g., small diameter inlays used to alleviate effects of presbyopia. For the purposes of the presented experiment, however, the entrance pupil diameter remained fixed at 4.5 mm.

Regarding visual testing, we found that the highly myopic subjects, once corrected of defocus and astigmatism, achieved normal values of VA. However, the reduction in visual performance in high myopes has been reported before as a consequence of retinal stretching [54–56]. In a different study, it was also argued that the magnification of the retinal images due to the enlarged eye might compensate for insufficient sampling of the retinal photoreceptors [57]. In some cases, the reduced visual performance of the myopic eye can be explained in terms of the minification effect of correcting lenses, or even contact lenses introducing additional aberrations [54,55].

With the AOVS, however, such problems are eliminated because a virtually perfect correction can be applied at the pupil plane, which may explain the high VA results for most of the subjects. Keeping in mind the limited number of participants in the study, VA of corrected myopic eyes seems to be comparable to VA of emmetropic eyes. AO correction has been

previously employed to achieve higher VA values for both emmetropes and myopes [22,24,34,44]. As an example, in the work of Rossi *et al.* [44], decimal VA values of up to 1.7 were reported for some myopic subjects. The high VA values may also be attributed to different methods of VA calculation, as the threshold in the psychometric sigmoid used in the study was not provided. Taking that into account, measured VA values after HOA correction agreed with previously reported in the literature.

The low VA values obtained by subjects S1 to S4, when looking through their prescribed corrections, are quite remarkable. These findings might be a consequence of the difficulty in obtaining an accurate refraction for high myopes using the trial lenses in the standard optometric procedure. The instrument presented here offers an alternative for obtaining the refraction for any patient, while also being faster and more precise. Astigmatism appears to be the potential cause of low VA with prescribed refraction in some cases. The objective procedure based on the HS measurements provides a near-perfect estimation of both orientation and magnitude, helping to attain higher VA values.

Regarding the correction of HOA, we have found a general visual benefit to the VA, even if modest. Since the amount of HOA for a 4.5 mm pupil is relatively low, the impact of this correction is limited. For larger pupils and eyes affected by higher HOA, the correction of such aberration can be substantial.

In summary, a novel AOVS with extended dioptric range has been developed and tested in a group of subjects.

Funding. Horizon 2020 Framework Programme (H2020) (675137); H2020 European Research Council (ERC) (ERC-2013-AdG-339228); Fundación Séneca (f SéNeCa) (19897/GERM/15); Secretaría de Estado de Investigación, Desarrollo e Innovación (SEIDI) (FIS2016-76163-R); European Regional Development Fund (ERDF) (EU-FEDER); Fundación Séneca (f SéNeCa) (20513/PDC/18).

Acknowledgment. The authors thank Javier Roca for developing parts of the software for controlling the instrument.

REFERENCES

1. K. Rose, W. Smith, I. Morgan, and P. Mitchell, "The increasing prevalence of myopia: implications for Australia," Clin. Exp. Ophthalmol. **29**, 116–120 (2001).
2. C.-W. Pan, M. Dirani, C.-Y. Cheng, T.-Y. Wong, and S.-M. Saw, "The age-specific prevalence of myopia in Asia: a meta-analysis," Optom. Vis. Sci. **92**, 258–266 (2015).
3. B. A. Holden, T. R. Fricke, D. A. Wilson, M. Jong, K. S. Naidoo, P. Sankaridurg, T. Y. Wong, T. J. Naduvilath, and S. Resnikoff, "Global prevalence of myopia and high myopia and temporal trends from 2000 through 2050," Ophthalmology **123**, 1036–1042 (2016).
4. J. Liang, B. Grimm, S. Goelz, and J. F. Bille, "Objective measurement of wave aberrations of the human eye with the use of a Hartmann-Shack wave-front sensor," J. Opt. Soc. Am. A **11**, 1949–1957 (1994).
5. J. Liang and D. R. Williams, "Aberrations and retinal image quality of the normal human eye," J. Opt. Soc. Am. A **14**, 2873–2883 (1997).
6. P. M. Prieto, F. Vargas-Martn, S. Goelz, and P. Artal, "Analysis of the performance of the Hartmann-Shack sensor in the human eye," J. Opt. Soc. Am. A **17**, 1388–1398 (2000).
7. J. Porter, A. Guirao, I. G. Cox, and D. R. Williams, "Monochromatic aberrations of the human eye in a large population," J. Opt. Soc. Am. A **18**, 1793–1803 (2001).
8. H. Hofer, P. Artal, B. Singer, J. L. Aragón, and D. R. Williams, "Dynamics of the eye's wave aberration," J. Opt. Soc. Am. A **18**, 497–506 (2001).
9. M. P. Cagigal, V. F. Canales, J. F. Castejón-Mochón, P. M. Prieto, N. López-Gil, and P. Artal, "Statistical description of wave-front aberration in the human eye," Opt. Lett. **27**, 37–39 (2002).
10. L. N. Thibos, X. Hong, A. Bradley, and X. Cheng, "Statistical variation of aberration structure and image quality in a normal population of healthy eyes," J. Opt. Soc. Am. A **19**, 2329–2348 (2002).
11. A. Mira-Agudelo, L. Lundström, and P. Artal, "Temporal dynamics of ocular aberrations: monocular vs binocular vision," Ophthalmic Physiolog. Opt. **29**, 256–263 (2009).
12. E. Chirre, P. M. Prieto, and P. Artal, "Binocular open-view instrument to measure aberrations and pupillary dynamics," Opt. Lett. **39**, 4773–4775 (2014).
13. J. Liang, D. R. Williams, and D. T. Miller, "Supernormal vision and high-resolution retinal imaging through adaptive optics," J. Opt. Soc. Am. A **14**, 2884–2892 (1997).
14. H. Hofer, L. Chen, G. Y. Yoon, B. Singer, Y. Yamauchi, and D. R. Williams, "Improvement in retinal image quality with dynamic correction of the eye's aberrations," Opt. Express **8**, 631–643 (2001).
15. N. Doble, G. Yoon, L. Chen, P. Bierden, B. Singer, S. Olivier, and D. R. Williams, "Use of a microelectromechanical mirror for adaptive optics in the human eye," Opt. Lett. **27**, 1537–1539 (2002).
16. E. J. Fernández and P. Artal, "Membrane deformable mirror for adaptive optics: performance limits in visual optics," Opt. Express **11**, 1056–1069 (2003).
17. D. T. Miller, L. N. Thibos, and X. Hong, "Requirements for segmented correctors for diffraction-limited performance in the human eye," Opt. Express **13**, 275–289 (2005).
18. E. Dalimier and C. Dainty, "Comparative analysis of deformable mirrors for ocular adaptive optics," Opt. Express **13**, 4275–4285 (2005).
19. E. J. Fernández, A. Unterhuber, B. Považay, B. Hermann, P. Artal, and W. Drexler, "Chromatic aberration correction of the human eye for retinal imaging in the near infrared," Opt. Express **14**, 6213–6225 (2006).
20. E. J. Fernández and P. Artal, "Ocular aberrations up to the infrared range: from 6328 to 1070 nm," Opt. Express **16**, 21199–21208 (2008).
21. E. J. Fernández, P. M. Prieto, and P. Artal, "Binocular adaptive optics visual simulator," Opt. Lett. **34**, 2628–2630 (2009).
22. P. A. Piers, N. E. Sverker Norrby, and U. Mester, "Eye models for the prediction of contrast vision in patients with new intraocular lens designs," Opt. Lett. **29**, 733–735 (2004).
23. S. Manzanera, P. M. Prieto, D. B. Ayala, J. M. Lindacher, and P. Artal, "Liquid crystal adaptive optics visual simulator: application to testing and design of ophthalmic optical elements," Opt. Express **15**, 16177–16188 (2007).
24. C. Cánovas, P. M. Prieto, S. Manzanera, A. Mira, and P. Artal, "Hybrid adaptive-optics visual simulator," Opt. Lett. **35**, 196–198 (2010).
25. P. Artal, L. Chen, E. J. Fernández, B. Singer, S. Manzanera, and D. R. Williams, "Neural compensation for the eye's optical aberrations," J. Vis. **4**(4), 281–287 (2004).
26. E. J. Fernández, A. Unterhuber, P. M. Prieto, B. Hermann, W. Drexler, and P. Artal, "Ocular aberrations as a function of wavelength in the near infrared measured with a femtosecond laser," Opt. Express **13**, 400–409 (2005).
27. P. A. Piers, S. Manzanera, P. M. Prieto, N. Gorceix, and P. Artal, "Use of adaptive optics to determine the optimal ocular spherical aberration," J. Cataract Refractive Surg. **33**, 1721–1726 (2007).
28. L. Lundström, S. Manzanera, P. M. Prieto, D. B. Ayala, N. Gorceix, J. Gustafsson, P. Unsbo, and P. Artal, "Effect of optical correction and remaining aberrations on peripheral resolution acuity in the human eye," Opt. Express **15**, 12654–12661 (2007).
29. P. Artal, S. Manzanera, P. Piers, and H. Weeber, "Visual effect of the combined correction of spherical and longitudinal chromatic aberrations," Opt. Express **18**, 1637–1648 (2010).

30. E. J. Fernández, P. M. Prieto, and P. Artal, "Adaptive optics binocular visual simulator to study stereopsis in the presence of aberrations," J. Opt. Soc. Am. A **27**, A48–A55 (2010).
31. E. J. Fernández, "Adaptive optics for visual simulation," ISRN Opt. **2012**, 1–13 (2012).
32. E. A. Villegas, E. Alcón, S. Mirabet, I. Yago, J. M. Marín, and P. Artal, "Extended depth of focus with induced spherical aberration in light-adjustable intraocular lenses," Am. J. Ophthalmol. **157**, 142–149 (2014).
33. S. Manzanera and P. Artal, "Minimum change in spherical aberration that can be perceived," Biomed. Opt. Express **7**, 3471–3477 (2016).
34. E. J. Fernández, P. M. Prieto, and P. Artal, "Wave-aberration control with a liquid crystal on silicon (LCOS) spatial phase modulator," Opt. Express **17**, 11013–11025 (2009).
35. F. Vargas-Martn, P. M. Prieto, and P. Artal, "Correction of the aberrations in the human eye with a liquid-crystal spatial light modulator: limits to performance," J. Opt. Soc. Am. A **15**, 2552–2562 (1998).
36. P. M. Prieto, E. J. Fernández, S. Manzanera, and P. Artal, "Adaptive optics with a programmable phase modulator: applications in the human eye," Opt. Express **12**, 4059–4071 (2004).
37. J. Primot, "Theoretical description of Shack-Hartmann wave-front sensor," Opt. Commun. **222**, 81–92 (2003).
38. E. J. Fernández and P. Artal, "Study on the effects of monochromatic aberrations in the accommodation response by using adaptive optics," J. Opt. Soc. Am. A **22**, 1732–1738 (2005).
39. B. Wang and K. J. Ciuffreda, "Depth-of-focus of the human eye: theory and clinical implications," Surv. Ophthalmol. **51**, 75–85 (2006).
40. T. O. Salmon and C. van de Pol, "Normal-eye Zernike coefficients and root-mean-square wavefront errors," J. Cataract Refractive Surg. **32**, 2064–2074 (2006).
41. J. L. M. Fuentes, E. J. Fernández, P. M. Prieto, and P. Artal, "Interferometric method for phase calibration in liquid crystal spatial light modulators using a self-generated diffraction-grating," Opt. Express **24**, 14159–14171 (2016).
42. M. Bach, "The Freiburg visual acuity test–automatic measurement of visual acuity," Optometry Vis. Sci. **73**, 49–53 (1996).
43. A. Dehnert, M. Bach, and S. P. Heinrich, "Subjective visual acuity with simulated defocus," Ophthalmic Physiolog. Opt. **31**, 625–631 (2011).
44. E. A. Rossi, P. Weiser, J. Tarrant, and A. Roorda, "Visual performance in emmetropia and low myopia after correction of high-order aberrations," J. Vis. **7**(8), 14 (2007).
45. X. Cheng, A. Bradley, X. Hong, and L. N. Thibos, "Relationship between refractive error and monochromatic aberrations of the eye," Optometry Vis. Sci. **80**, 43–49 (2003).
46. M. P. Paquin, H. Hamam, and P. Simonet, "Objective measurement of optical aberrations in myopic eyes," Optometry Vis. Sci. **79**, 285–291 (2002).
47. J. C. He, P. Sun, R. Held, F. Thorn, X. Sun, and J. E. Gwiazda, "Wavefront aberrations in eyes of emmetropic and moderately myopic school children and young adults," Vis. Res. **42**, 1063–1070 (2002).
48. M. J. Collins, C. F. Wildsoet, and D. A. Atchison, "Monochromatic aberrations and myopia," Vis. Res. **35**, 1157–1163 (1995).
49. A. Carkeet, H. Dong Luo, L. Tong, S. M. Saw, and D. T. Tan, "Refractive error and monochromatic aberrations in Singaporean children," Vis. Res. **42**, 1809–1824 (2002).
50. C. Dorronsoro, A. Radhakrishnan, J. R. Alonso-Sanz, D. Pascual, M. Velasco-Ocana, P. Perez-Merino, and S. Marcos, "Portable simultaneous vision device to simulate multifocal corrections," Optica **3**, 918–924 (2016).
51. B. F. Grewe, F. F. Voigt, M. van't Hoff, and F. Helmchen, "Fast two-layer two-photon imaging of neuronal cell populations using an electrically tunable lens," Biomed. Opt. Express **2**, 2035–2046 (2011).
52. I. Grulkowski, S. Manzanera, L. Cwiklinski, F. Sobczuk, K. Karnowski, and P. Artal, "Swept source optical coherence tomography and tunable lens technology for comprehensive imaging and biometry of the whole eye," Optica **5**, 52–59 (2018).
53. World Health Organization–Brien Holden Vision Institute, The Impact of Myopia and High Myopia (2015).
54. J. Collins and L. Carney, "Visual performance in high myopia," Curr. Eye Res. **9**, 217–224 (1990).
55. N. C. Strang, B. Winn, and A. Bradley, "The role of neural and optical factors in limiting visual resolution in myopia," Vis. Res. **38**, 1713–1721 (1998).
56. T. Y. Chui, M. K. Yap, H. H. Chan, and L. N. Thibos, "Retinal stretching limits peripheral visual acuity in myopia," Vis. Res. **45**, 593–605 (2005).
57. N. J. Coletta and T. Watson, "Effect of myopia on visual acuity measured with laser interference fringes," Vis. Res. **46**, 636–651 (2006).